Materials Science in Semiconductor Processing 86 (2018) 93–100

Contents lists available at ScienceDirect

Materials Science in Semiconductor Processing

journal homepage: www.elsevier.com/locate/mssp

The role of the molar ratio of (HNO_3/Bi^{3+}) on the formation and morphology of α-Bi_2O_3 microrods with photocatalytic properties

Agileo Hernández-Gordillo*, Larisa Vazquez, Jesica Ramos, Monserrat Bizarro, Sandra E. Rodil

Instituto de Investigaciones en Materiales, Universidad Nacional Autónoma de México, Circuito Exterior SN, Ciudad Universitaria, CP 04510 México D.F., Coyoacán, México

ARTICLE INFO

Keywords:
Microrods α-Bi_2O_3
Ethylenediamine-solvent
Bismuth-Nitrate
Amorphous-sheet

ABSTRACT

Enlarged microrods α-Bi_2O_3 were directly obtained by chemical precipitation method at soft reflux conditions using ethylenediamine-solvent as precipitating and morphological template, in absence or presence of nitric acid. The influence of the molar ratio of HNO_3/Bi^{3+} (0, 5 and 10) and reflux temperature, maintaining fixed the Bi^{3+} content in solution, on the formation of Bi_2O_3 or amorphous-compounds was investigated. The structure and properties of the α-Bi_2O_3 obtained by the direct precipitation condition or after calcination were obtained by X-ray diffraction, infrared analysis, diffuse reflectance spectroscopy and scanning electron microscopy. A relationship between the reflux temperature and the molar ratio of HNO_3/Bi^{3+} ions for the direct formation of α-Bi_2O_3 phase is discussed. The photocatalytic properties, recyclability and stability of α-Bi_2O_3 solids were tested in the photodegradation of indigo carmine dye under UV-Light. X-ray diffraction and infrared analysis of the reused α-Bi_2O_3 were also included.

1. Introduction

Bismuth oxide (Bi_2O_3) is a semiconductor material used in diverse applications such as ceramic glass, gas sensor, optical coatings and as a visible-light photocatalyst for indoor air or water purification due to their semiconducting optical and electrical properties [1–4]. Among all its crystallographic polymorphs, monoclinic α-Bi_2O_3 phase exhibit light absorption in the visible range of the solar spectrum (2.8 eV) and it has been used as photocatalysts to decompose organic pollutants by the photocatalytic process [5–8], where the improvement of charge separation and efficient interelectron transfer are the key factors for enhancing the photocatalytic activity. The special photocatalytic properties of bismuth based materials are related to their well-defined-morphologies, since this is an essential factor to define their activity, while its preparation is feasible by adjusting the reaction conditions [9]. The properties are influenced by the synthesis method; hydrothermal [10,11], microwave [12,13], sonochemical [8] or precipitation method [14–16] and in some cases is also affected by the annealing conditions [7]. For example, monoclinic α-Bi_2O_3 (the room temperature stable phase) obtained by a sustainable green synthesis method showed changes on the textural properties as a consequence of variations in aging time or annealing conditions [17,18]. Among the chemical synthesis methods, room-temperature precipitation is considered an easy and economic method for the preparation of bismuth based materials (Bi_2O_3, $BiVO_4$, $BiMoO_6$, $BiWO_6$) leading to a variety of morphologies [16,19–21].

For the preparation of the monoclinic α-Bi_2O_3 phase bismuth nitrate $Bi(NO_3)_3$ is the bismuth precursor typically employed in the presence of nitric acid (HNO_3), giving a molar ratio of HNO_3/Bi^{3+} ions from 1 to 8, but the crystalline structure, the composition, the crystal growth and morphology are strongly influenced by the type of; a) the organic additive (PVV [12], PEGX000 [17], oleic acid [22], glycerin [15]); and b) the inorganic precipitating agent (NaOH, NH_4OH, KOH). In the later case, it has been showed that an appropriate molar ratio of HNO_3/OH^- ions from 5 to 16 should be used to neutralize the acid and get a uniform precipitation [16]. The results suggest that elongated one-dimensional particles of Bi_2O_3 along the [001] direction are obtained at high concentrations of nitrate (NO_3^-) ions; while the preferred crystal growth direction is influenced by the concentration of hydroxyl (OH^-) ions [8,13,16,19].

As a novel alternative chemical synthesis, it is possible to neutralize the nitric acid by using amine cations ($ENH_2^{2+} \leftrightarrow ENH^+$) in equilibrium from a *diamine-solvent* [23], where the Bi^{3+} ions can be precipitated forming different complexes [24–27] or the α-Bi_2O_3 phase, depending on the synthesis conditions [20,28]. In this line, we have previously reported the preparation of enlarged-individual α-Bi_2O_3 microrods in soft synthesis condition (boiling point), varying the ethylenediamine concentration (*ENH^+-solvent*) in the interval of 20–50 vol%. Depending

* Corresponding author.
E-mail addresses: agileo12@hotmail.com, agileohg@iim.unam.mx (A. Hernández-Gordillo).

https://doi.org/10.1016/j.mssp.2018.06.024
Received 23 January 2018; Received in revised form 20 June 2018; Accepted 24 June 2018
Available online 02 July 2018
1369-8001/

on the $ENH_2^{2+} \leftrightarrow ENH^+$ content, the α-Bi_2O_3 microrods grew along one-direction with a homogeneous shape and uniform-size [29]. It was shown that the *ENH^+-solvent* facilitates the nucleation and accelerate the precipitation reaction of Bi^{3+} ions into α-Bi_2O_3 during the reflux condition. One of the –NH_2 groups of *ENH^+-solvent* attach onto the growing nanocrystals, inducing the formation of the enlarged microrods. The precipitation occurs in the presence of nitric acid (HNO_3), however, the role of the nitrate (NO_3^-) ions and amine ($ENH_2^{2+} \leftrightarrow ENH^+$) cations on the formation of α-Bi_2O_3 microrods during the precipitation was not fully understood. Moreover, the effect of different reflux conditions were not explored and it is very well-known that thermal treatment of precipitated solids by reflux is the most classic way to obtain oxides and depending on the temperature, the reflux treatment can affect the physicochemical (morphology and crystalline) properties of the material, obtaining large particle aggregation or mixture of compounds. For example during the preparation of Bi_2WO_6 in the presence of *ENH^+-solvent,* the transformation from Bi_2O_3 to Bi_2WO_6 was favored by increasing the reaction temperature up to 150 °C, while at lower temperature, Bi_2O_3 was obtained [28].

Therefore, in order to gain new information about the role of the nitric acid or the reflux temperature, we studied the influence of the molar ratio HNO_3/Bi^{3+} or HNO_3/ENH^+ on the formation of Bi_2O_3 solid, using *ENH^+-solvent* as precipitating and morphological template, under soft synthesis conditions, but also evaluated the influence of the reflux temperature (50–80 °C). Microstructures of Bi_2O_3 using molar ratio of $HNO_3/OH^- = 0.4$ at 80 °C were also prepared for comparison. In addition, the structure and photoactivity properties of the precipitated powders after calcination were also evaluated. All solids were characterized by diverse techniques and the role of the molar ratio HNO_3/Bi^{3+} or HNO_3/ENH^+ on the transformation mechanism of nanocrystalline α-Bi_2O_3 solid is discussed. The physicochemical properties of Bi_2O_3 were correlated with the adsorption capacity and photocatalytic properties in the photodegradation of indigo carmine (*IC*) dye. TOC analysis, recyclability and photostability test of the two Bi_2O_3 solids was also investigated.

2. Materials and methods

2.1. Synthesis of the Bi_2O_3

The Bi_2O_3 solids were synthesized by a chemical precipitation method using Ethylenediamine-solvent in aqueous solution (40 vol% *ENH^+-solvent*) as precipitating agent [29], under different reflux conditions (50–80 °C). The Bi^{3+} concentration in aqueous solution was fixed at 41 mM and two concentrations of nitric acid (HNO_3) were used: 0.2 and 0.4 M, leading to molar ratio of $HNO_3/Bi^{3+} = 5$ and 10, respectively, (see Table 1). Through a typical procedure, $Bi(NO_3)_3{\cdot}5H_2O$ (Aldrich) were dissolved in the appropriate HNO_3 solution at ~ 40 °C under constant stirring and the transparent Bi^{3+} solution was cooled at room temperature. Afterwards, the *ENH^+-solvent* (Aldrich) was added drop wise into Bi^{3+} solution, leading to fixed molar ratio of $ENH^+/Bi^{3+} = 241$ and the precipitated suspension was reflux at 50 °C under vigorous magnetic stirring (800 RPM) for 2 h. Subsequently it was cooled at room temperature (RT) and the resulting precipitated solid was collected by filtration, washed using an ethanol-water solution and left to dry at RT. Additional, Bi_2O_3 solids were also prepared without the addition of HNO_3 solution, i. e. $HNO_3/Bi^{3+} = 0$. In this case, the Bi $(NO_3)_3{\cdot}5H_2O$ was added in water, the *ENH^+-solvent* was immediately added drop wise and the suspension was refluxed at room temperature (RT) and 50 °C, following the procedure described above (Table 1).

Table 1
Data of synthesis condition and name of the solids.

Sample	HNO_3 [M]	Ratio HNO_3/Bi^{3+}	Ratio HNO_3/ENH^+	Reflux temp (°C)
$NB0_{RT}$	0.00	00	–	~ 25 °C
NB0	0.00	00	–	50
NB5	0.20	05	0.02	50
NB10	0.40	10	0.04	50
$NB10_{T7}$	0.40	10	0.04	70
$NB10_{T8}$	0.40	10	0.04	80
NB10-OH	0.26	10	*0.4 (OH)	80

* Molar ratio $HNO_3/OH^- = 0.4$, using 10 mL of NaOH (10 M), respectively.

The obtained solids were labeled as **NBX**, where NB represents the $[HNO_3/Bi^{3+}]$ molar ratio and X represent the value (0, 5 and 10).

In order to study the influence of the reflux temperature, Bi_2O_3 solids were obtained using the molar ratio of $[HNO_3/Bi^{3+} = 10]$ following the same procedure but changing the temperature of reflux to 70 and 80 °C. The obtained solids were labeled as **$NB10_{TY}$**, where T represent the temperature of reflux and Y represent the value (70 and 80). Some selected as-prepared solids were annealed at 600 °C in static air for 1 h, using a heating rate of 10 °C/min and they were labeled adding the letter C, i.e. **NB10C** and **$NB10_{T7}C$**. Separately, for comparison effect, one Bi_2O_3 solid was prepared using 10 mL of NaOH (10 M) as the precipitating agent, leading to molar ratio $HNO_3/OH^- = 0.4$, reflux at 80 °C and labeled as **NB10-OH**.

2.2. Characterization of the Bi_2O_3

The obtained Bi_2O_3 solids were characterized by powder X-ray diffraction using a SIEMENS D500 diffractometer with Cu Kα radiation of 0.15406 nm (34 kV, 25 mA). The scanning range was between 20° and 60° (2 theta) with a step size of 0.013°/s. For the lattice parameter determination, the Bragg law was used considering a monoclinic structure for the alpha phase. The average crystal size was obtained using the Halder-Wagner method in the PDXL2 software by the following expression: $\left(\frac{\beta^*}{d^*}\right)^2 = \frac{1}{D}\frac{\beta^*}{(d^*)^2} + \left(\frac{\varepsilon}{2}\right)^2$, assuming a Voigtian peak shape, where the crystallite size (D) and the strain (ε) are related to β*. From above equation, the intercept of the plot of $(\beta^*/d^*)^2$ versus $\beta^*/(d^*)^2$, gives the value of the equivalent strain and the slope gives the value of the crystallite size [30]. The morphology of the solids was revealed by scanning electron microscopy (SEM) using a JEOL 7600F operated at 10 kV. The UV–Vis diffuse reflectance spectra (DRS) were recorded on a UV–Vis spectrophotometer (Shimadzu 2600) equipped with an integration sphere (ISR 2600) in the range of 190 and 800 nm and using $BaSO_4$ as a reference blank. The spectra were converted from reflectance to absorbance by the Kubelka–Munk method. The band-gap energy (E_g) was calculated considering an allowed direct transition for α-Bi_2O_3 phase [31], by extrapolating the linear portion of the $(F(R) \times h\nu)^2$ *vs* $h\nu$ curves to $F(R) = 0$ [11]. The FTIR absorption spectra of all the samples were recorded on a Thermoscientific Nicolet 6700 spectrometer using an attenuated total reflection (ATR) accessory provided of a diamond crystal. For each measurement, the powder was loaded and the pressure used was of 815 Psi. Typically, 34 scans at a resolution of 4 cm^{-1} in the range between 500 and 4000 cm^{-1} in the transmittance mode were used for the measurements at room temperature. Thermal analysis (DSC/TGA) of selected as-prepared solid was performed up to 800 °C at a heating rate of 10 °C/min in static air atmosphere using a TA Instruments SDT Q600 V8.3 Build 101.

2.3. Photodegradation of indigo carmine (IC) dye

The photodegradation reaction was performed in an open-air-glass-photoreactor system containing 200 mL of an aqueous solution with 5 ppm of *IC* dye and 0.30 g/L of the photocatalyst powder load. The exposed-to-air suspension was maintained under magnetic stirring at 1000 RPM, at room temperature and without any pH adjustment (natural pH = 7). The system was irradiated by means of a UV lamp of 9 W (maximum emitting light at λ = 367 nm, irradiance of 26 Wm^{-2},) placed into the suspension. Before irradiation, the suspension was kept

under dark conditions for 30 min to ensure the adsorption-desorption equilibrium. In all cases, the estimation of the *IC* dye concentration was done by taking a filtered aliquot of 3 mL at time intervals and analyzing the aliquot absorbance (absorption band at 610 nm for *IC*) using UV–Vis spectroscopy on a Shimadzu 1800 spectrometer. The reaction kinetic was established by considering the Langmuir–Hinshelwood kinetic model, usually applicable to describe the photodegradation kinetics on semiconductors [29]. The total organic carbon of the irradiated solution was determined by using a TOC-L Shimadzu Total Organic Carbon analyzer by using NPOC method in high sensibility mode. Water containing 1 ppb of carbon (Zerowater, from Shimadzu) was used for the samples preparation. Recyclability test was performed for the two Bi_2O_3 solids, using an aqueous solution with 10 ppm of *IC* dye and 0.30 g/L of the photocatalyst powder load, evaluated at 1 and 2 h of reaction. After each reaction, the photocatalyst powder was recovered by decantation and it was used again to degrade the 10 ppm of *IC* dye, this was repeated 4 times.

3. Results and discussion

3.1. Crystalline structure of solids

The X-ray diffraction patterns of solids prepared at different molar ratio of HNO_3/Bi^{3+} ions and reflux at 50 °C are shown in the Fig. 1A. For the solid prepared without addition of nitric acid, the pattern of the solid refluxed at room temperature is also included (**$NB0_{RT}$**). Both **NB0** solids exhibited reflection peaks at 26.9, 27.4, 28.0, 33.2 and 46.3° in 2θ, corresponding to principal planes (002), (111), (120), (012), (-122, 200) and (041), respectively, indexed to the monoclinic structure of α-Bi_2O_3 phase (JCPDS card no. 01-041-1449) [10]. This demonstrate that the crystalline monoclinic structure is already obtained at room temperature without the addition of HNO_3 and similar structure was obtained at 50 °C. It suggests that the basic bismuth nitrate compound was directly converted to α-Bi_2O_3 phase when entered in contact with the *ENH^+-solvent*. It is known that in low concentrations of HNO_3 solution, the bismuth precursor ($Bi(NO_3)_3{\cdot}5H_2O$) is immediately hydrolyzed in contact with water, forming the basic bismuth nitrate [$Bi_6O_5(OH)_3(NO_3)_5(H_2O)_3$] compound [16], however, reflection peaks of either bismuth precursor or basic bismuth nitrate were not detected. The solid prepared using a molar ratio of HNO_3/Bi^{3+} = 5 at 50 °C (**NB5** solid) exhibited reflection peaks of the planes (120), (200) and (041), characteristic of the α-Bi_2O_3 phase, however, comparing to the **NB0** solid, the reflection peaks are wider and fewer, suggesting poor crystallinity. Increasing the molar ratio of HNO_3/Bi^{3+} to 10, the **NB10** solid exhibited a wide peak from 25° to 35°, centered at ~ 28.3° in 2θ, suggesting that the as-prepared solid is nanocrystalline or XRD-amorphous (Fig. 1A). This indicates that at high amount of HNO_3, the *ENH^+-solvent* is not capable to carry out the conversion of bismuth precursor toward Bi_2O_3 oxide. In this case, a new amorphous-compound, not identified, was formed..

To understand the role played by the HNO_3 and the temperature of reflux in the formation mechanism of Bi_2O_3, the X-ray diffraction patterns of solids prepared at molar ratio of HNO_3/Bi^{3+} = 10 and reflux at 70 and 80 °C are shown in the Fig. 1B. At temperature of 70 °C, the **$NB10_{T7}$** solid showed the wide amorphous-like band overlapped with two small peaks in 2θ corresponding to the planes (120) and (200) of α-Bi_2O_3 phase. This indicates the presence of both amorphous-compound and α-Bi_2O_3 phase. Increasing the temperature at 80 °C, the **$NB10_{T8}$** solid exhibited well-defined reflection peaks characteristic of the α-Bi_2O_3 phase. The amorphous-compound was suppressed, suggesting that the conversion to α-Bi_2O_3 phase was complete. Similarly to the **NB0** solids, the peak corresponding to the (120) plane of α-Bi_2O_3 phase is the most intense, which is typical of the α-Bi_2O_3 phase [12]. By applying the Halder-Wagner method, the average grain size of α-Bi_2O_3 crystals are between 20 and 22 nm.

For comparison effect, α-Bi_2O_3 phase was also prepared at molar ratio of HNO_3/Bi^{3+} = 10, but using OH^- ions as precipitating agent and reflux at 80 °C. The X-ray diffraction pattern of **NB10OH** solid is shown in Fig. 1B. This solid exhibited reflection peaks corresponding to the monoclinic structure of α-Bi_2O_3 phase, however, its reflection peaks are wider, suggesting that the crystal size is smaller than those precipitated using the *ENH^+-solvent*. It is known that high concentrations of OH^- ions neutralize to HNO_3 to achieve the complete crystallization of α-Bi_2O_3 phase [16].

3.2. Morphology of solids

The SEM image of the six solids are presented in the Fig. 2. The sequence at the top shows the effect of the different molar ratio of HNO_3/Bi^{3+} ions in the morphology. Without the addition of HNO_3 solution, the Bi_2O_3 solid showed enlarged microrods-like morphology of diverse dimensions, with lengths (*L*) of 3–5 μm and the diameters (*D*) between 0.3 and 1.5 μm. It indicates that *ENH^+-solvent* also directly acts as a morphological-structuring agent, inducing the unidirectional formation of Bi_2O_3 microrods. For the **NB5** solid, the addition of small HNO_3 contents, affected the dimensions and type of morphology of the nanoparticles. In this case, rods, needles- and sheet-like particles in microsized (1–5 μm) and nanosized (0.1–0.3 μm) regime were formed, leading to a more heterogeneous morphology. When the concentration of HNO_3 is increased (molar ratio of HNO_3/Bi^{3+} = 10), the amorphous **NB10** solid exhibited huge microparticles of sheet-like morphology of large dimensions, where their lengths (*L*) can reach 5–20 μm and the

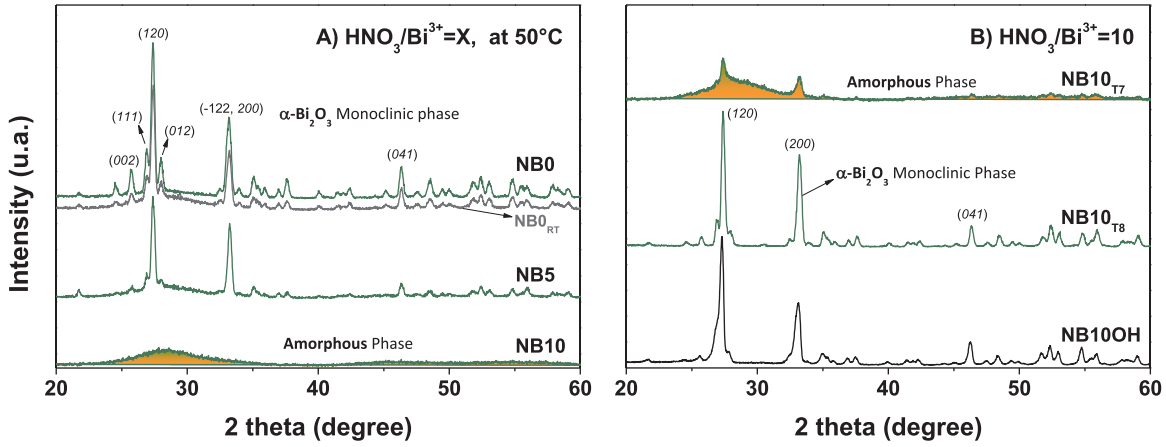

Fig. 1. XRD of solids prepared in *ENH^+-solvent*; A) different molar ratio of HNO_3/Bi^{3+} ions at 50 °C and B) different temperature of reflux at molar ratio of HNO_3/Bi^{3+} = 10 and the sample produced with OH^- ions.

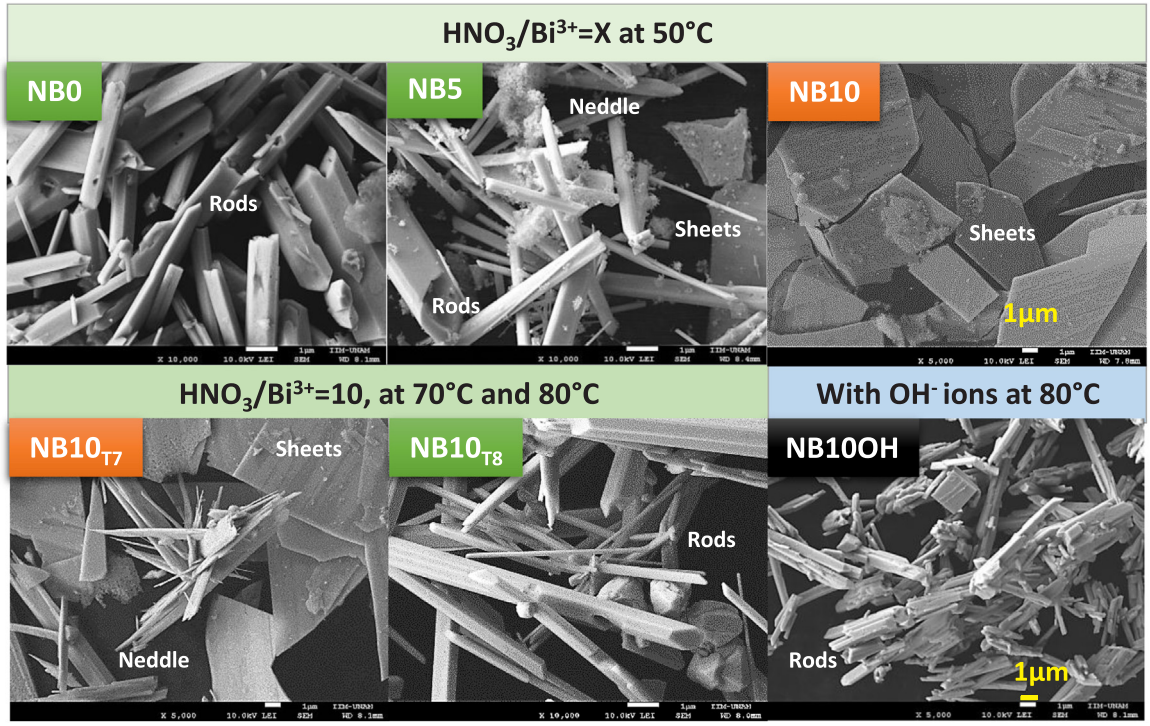

Fig. 2. SEM image of α-Bi_2O_3 solid precipitated with *ENH*$^+$*-solvent* at different molar ratio of HNO_3/Bi^{3+} (top) and different reflux temperature (bottom). α-Bi_2O_3 solid precipitated with OH^- ions at 80 °C is also included.

thickness (*th*) is approximately of ~ 0.1 μm. This is the sample that according to the XRD appeared as amorphous-like.

The bottom Fig. 2 shows the effect of the reflux temperature on the morphology of the samples. When the **NB10** sample is refluxed at 70 °C, the **NB10$_{T7}$** solid still exhibits huge microsheet particles, however, heterogeneous particles of needle-like morphology in micro-nanosized (0.1–0.5 μm) regime were also observed, which are probably related to the diffraction peaks found on top of the broad XRD signal. At temperature of 80 °C, the **NB10$_{T8}$** solid showed again enlarged microrod-like morphology of large dimensions, with lengths of 3–5 μm and diameters (*D*) between 0.8 and 1 μm. This microrod-morphology is characteristic of α-Bi_2O_3 when it is formed in presence of relative high content of *ENH*$^+$*-solvent* [29]. Conversely, the solid precipitated with OH^- ions (Fig. 2), **NB10OH,** exhibited short microrods of 3–4 μm, agglomerated in huge particles. It is known that the type of morphology and the dimensions of α-Bi_2O_3 microrods strongly depends of the molar ratio HNO_3/OH^-, as has been already reported [16].

By using *ENH*$^+$*-solvent* as precipitating agent, the type of morphology is related to the molar ratio of $HNO_3/Bi^{3+}/ENH^+$ ions. The needle- and rod-like particles are mainly composed by α-Bi_2O_3 crystals with a preferential orientation in the (*200*) plane, whereas the huge microsheet-like particles are a result of the agglomeration of amorphous-compounds. The one-directional growth of the amorphous-compound was only achieved at high molar ratio of HNO_3/Bi^{3+} = 10 and reflux temperature lower than 70 °C, but at higher reflux temperature the amorphous-compound is transformed into α-Bi_2O_3 phase. Therefore, the formation of α-Bi_2O_3 phase can be achieved from either basic bismuth nitrate or the amorphous-compound, depending on the entropy energy (Fig. 3). At molar ratio of HNO_3/Bi^{3+} below 5, the bismuth precursor is hydrolyzed forming the basic bismuth nitrate [16] and the addition of 40%vol. of amine-solvent ($ENH_2^{2+} \leftrightarrow ENH^+$) cause the direct conversion to α-Bi_2O_3 phase from room temperature. Indeed, α-Bi_2O_3 phase is well crystallized by increasing the temperature of reflux. On the other hand, increasing the molar ratio of HNO_3/Bi^{3+} = 10, high amount of NO_3^- ions interacts with the bismuth precursor, avoiding its hydrolyzation, then, the Bi^{3+} ions remained in the aqueous

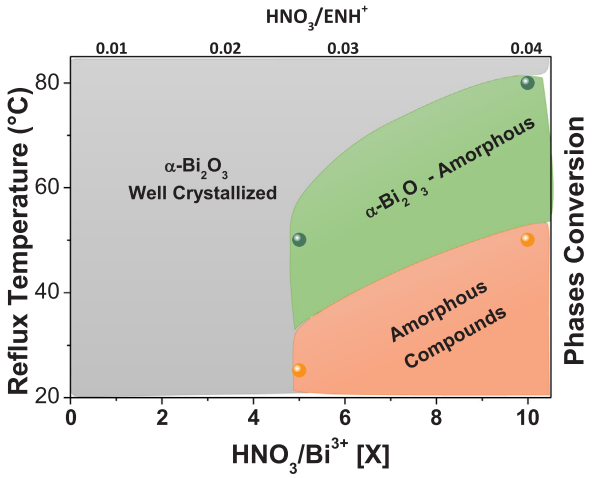

Fig. 3. Relationship of reflux temperature and molar ratio of HNO_3/Bi^{3+} ions for the direct conversion of either bismuth precursor or amorphous phase to α-Bi_2O_3 phase.

solution [19]. After the addition of the amine-solvent, a new solid is precipitated, which looks XRD-amorphous (very broad peaks), but consist of large micro-sheet particles. This amorphous-compound might be formed due to the strong coordination of the protonated amine cations with the Bi^{3+}-NO_3^- species, resulting in a possible anionic bismuthate layer, with the formula $(H_2en)_{0.5}[BiO(OH)_2(H_2O)]$ (en = -ethylenediamine), where the $ENH_2^{2+} \leftrightarrow ENH^+$ species are intercalated between two layers of BiO_8 dodecahedrons [25]. Indeed, this amorphous-compound is very stable at temperature of reflux below of 70 °C. By increasing the entropy energy up to 80 °C, the coordination of amine-BiO_8 in the amorphous-compound is weakened and the BiO_8 dodecahedrons are released, continuing to be converted into the α-Bi_2O_3 phase. The interaction of one of the –NH_2 groups of the *ENH*$^+$-solvent attached to the growing nanocrystals cap some facets of the α-

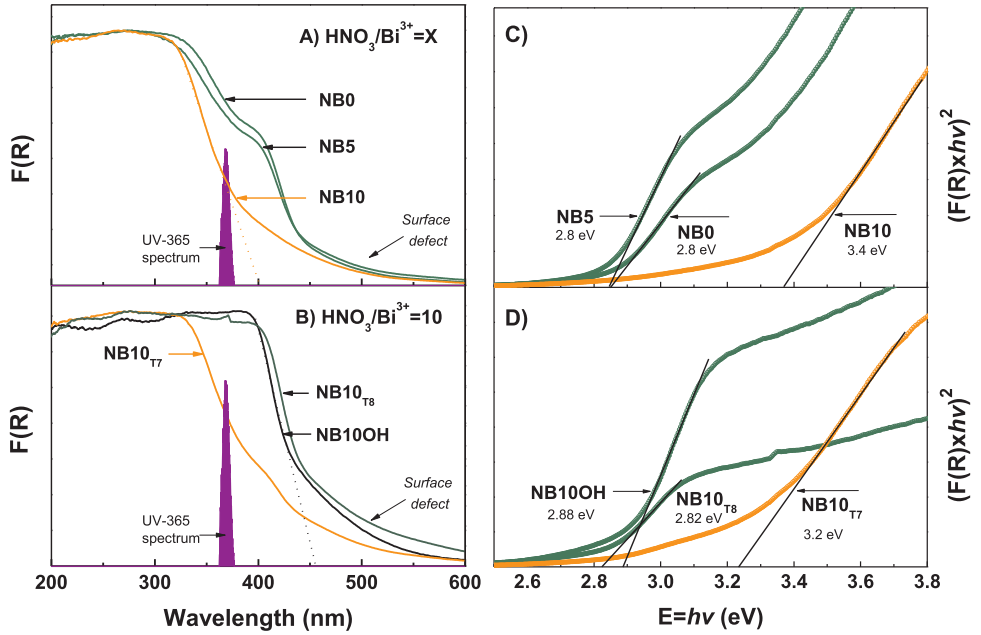

Fig. 4. (A, B) Diffuse reflectance spectra (emission spectrum of the UV-lamp is inset) and (C, D) optical band gap estimation of the amorphous-compound and α-Bi_2O_3 phase.

Bi_2O_3 crystals, resulting in the formation of the needle- and rod-like particles. Therefore, the transformation of amorphous-compounds toward nanocrystalline α-Bi_2O_3 phase starts at 70 °C and its full crystallization occurs by increasing the temperature above 70 °C (Fig. 3).

3.3. Optical properties of solids

The optical properties of the amorphous-compound and α-Bi_2O_3 phase, analyzed by UV–Vis DRS using the Kubelka-Munk function, and the band-gap determination are presented in Figs. 4A-B and 4C-D, respectively. The amorphous-compounds (**NB10** and **$NB10_{T7}$**) exhibited wide absorption in the UV region from 400 to 300 nm, probably due to the electron transitions of Bi^{3+} complex. The well crystallized α-Bi_2O_3 solids (**NB0, NB5, NB10T8** and **NB10OH**) exhibited wide absorption from 380 to 600 nm. The main absorption from 450 to 380 nm (Fig. 4A-B) is assigned to the intrinsic absorption band of the α-Bi_2O_3 phase [12]; however, the visible-light absorption edge above 450 nm has been associated to electron transitions caused by the presence of surface crystal defects [31]. For the **$NB10_{T7}$** solid, a shoulder absorption at 400–450 nm was also observed, indicating the presence of α-Bi_2O_3 phase. The band gap energy value for the amorphous-compounds is about of 3.2 ± 0.2 eV and for the α-Bi_2O_3 solid is 2.8 ± 0.05 eV (Fig. 4C-D), which is characteristic of α-Bi_2O_3 phase [2]. The emission spectrum of the UV-lamp used for the photocatalytic reaction is inset in Fig. 4A-B, where it can be seen that all materials presenting the α-Bi_2O_3 phase have strong absorption in the UV region for its activation.

3.4. FTIR analysis of solids

The FTIR spectra of the amorphous-compound and α-Bi_2O_3 solids are shown in the Fig. 5. The adsorption bands of the amorphous-compound samples are distinctly different from typical α-Bi_2O_3 phase solids, probably due to the formation of the bismuthate complex in the amorphous samples. For the **NB5, NB10** and **$NB10_{T7}$** solids containing amorphous-compounds, the FTIR spectrum was similar among them, exhibiting a broad absorption band at 3356 cm^{-1} corresponding to stretching vibrations of OH- and the absorption band from 3000 to 2800 cm^{-1} is related to asymmetric stretching vibrations of N-H groups; the band at 1300 cm^{-1} is related to the stretching vibrations of

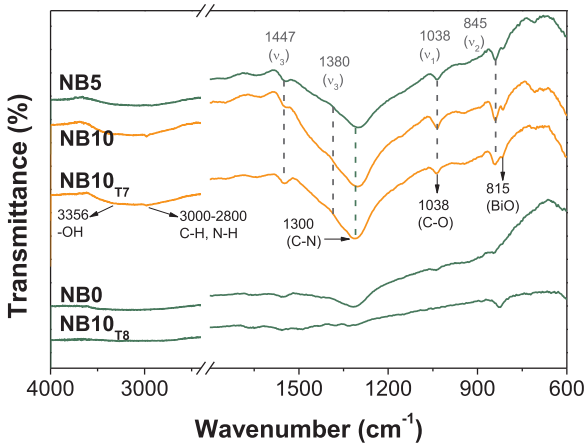

Fig. 5. FTIR analysis of the amorphous-compound and α-Bi_2O_3 phase solids.

CN- groups from the amine molecules [25]. On the other hand, the absorption bands at 1447, 1038 and 845 cm^{-1} are associated to the anti-symmetric vibrations (ν_3), symmetric stretching mode (ν_1) and out-of-plane bending mode (ν_2) of CO_3^{2-}, respectively. However, the absorption band of CO_3^{2-} at 1380 cm^{-1} is not observed or must be overlapped with the vibrations of CN- groups. There is a shift in the out-of-plane bending mode of CO_3^{2-} to 845 cm^{-1}, probably due to the interaction between the Bi–O bonds and their C–O surroundings, although it is smaller than that of the reference $(BiO)_2CO_3{*}H_2O$ [32,33]. The vibration bands of NH and CN groups suggest the presence of ethylenediamine molecule in the possible anionic bismuthate layer and the vibration peaks of CO_3^{2-} are possibly generated from the residual carbonate on the surface of bismuthate.

For the **NB0** and **$NB10_{T8}$** solids, the vibration bands of the formed bismuthate layer and the residual $(BiO)_2CO_3{*}H_2O$ disappear since both species were directly converted to α-Bi_2O_3 phase during the reflux treatment. The solids exhibited an adsorption band about 815 cm^{-1}, related with the vibrational band of Bi-O in bismuth oxide materials [34].

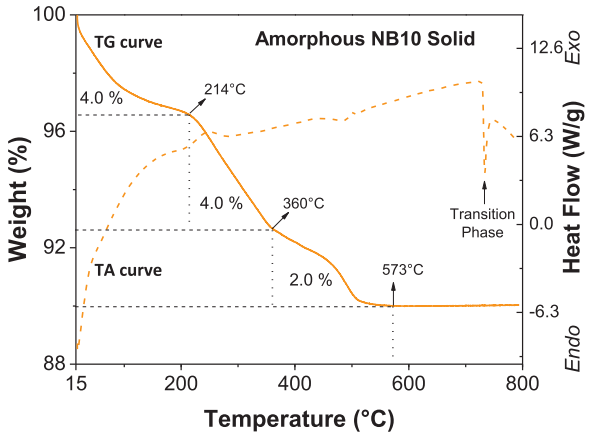

Fig. 6. TG and TA analysis of the amorphous-compound (**NB10** solid), prepared in a molar ratio of HNO_3/Bi^{3+} = 10 at 50 °C.

3.5. Annealing of amorphous-compound

The thermogravimetric analysis was made for the amorphous **NB10** solid (Fig. 6). The TG analysis exhibited three zones of weight loss, which occurred at temperatures of 30–214, 214–360 and 360–573 °C, corresponding to weight losses of 4.0% associated to the elimination of the physisorbed water, 4.0% related to the thermal decomposition of the organic compounds and 2.0 wt% due to the thermal decomposition of the nanocrystalline-complex or crystallization into Bi_2O_3, respectively [35]. Then, it remained stable up to 750 °C, where a transformation or phase transition without weight loss occurred, suggesting an endothermic event at this temperature. On basis of this, 600 °C was the selected temperature for annealing of amorphous-compound solid.

The X-ray diffraction patterns of the solids annealed at 600 °C are shown in Fig. 7A. It is observed that the annealed solids exhibited reflection peaks characteristic of α-Bi_2O_3 phase, without the presence of the broad XRD signal shown in Fig. 1. It indicates that the amorphous-compound is converted to α-Bi_2O_3 phase by a simple annealing at 600 °C. Interestingly the peaks associated to the planes (*200*) and (*041*), showed some variations in their relative intensity ratio, suggesting that depending on the reflux conditions, a different preferential orientation of the crystals was favored. For the **NB10-C** solid, the peak associated to the plane (*041*) is as intense as to the plane (*200*), but as the reflux temperature is increased up to 70 °C (**$NB10_{T7}$-C** solid), the intensity ratio is reversed, indicating that the preferred orientation has changed. It is not possible to estimate a texture coefficient since the (200) peak might be overlapped with other diffraction peaks such as (*-122*) or (202) plane [10]. However, this change in the intensity of both planes is related to the morphology and composition of the amorphous solid, which controls the α-Bi_2O_3 crystal growth depending on the reflux treatment. The average crystal sizes for all the annealed samples are between 22 and 27 nm.

On the other hand, the morphology of the α-Bi_2O_3 phase obtained by annealing the amorphous-compounds (Fig. 7B) is quite different to that obtained directly from basic bismuth nitrate. For the amorphous **NB10** solid, its microsheet structure (Fig. 2) was fully destroyed into heterogeneous small irregular particles of α-Bi_2O_3 phase with dimension in the interval of 0.5–2 μm (**NB10-C** solid). For the **$NB10_{T7}$** solid, its corresponding α-Bi_2O_3 phase (**$NB10_{T7}C$**) exhibited also heterogeneous microparticles as sheet-rod-like, exhibiting aspect of molten-like particles. These result show that by increasing the temperature of reflux during the synthesis of the amorphous-compound, the microsheets are hardly destroyed during the annealing process suggesting that the temperature promote the stabilization of the microsheets during the reflux process.

3.6. Photocatalytic activity of Bi_2O_3 solids

The photocatalytic properties of all α-Bi_2O_3 solids were evaluated in the photodegradation of indigo carmine (*IC*) dye under UV-light (367 nm). The absorbance spectrum of *IC* dye solution, after the adsorption and irradiation by using the **NB5** solid, is shown in the Fig. 8A. It exhibited the typical maximum absorbance peak at 610 nm, and it decreased during the UV-irradiation time, suggesting that its *indigoid group* was fully destroyed. It is known that using α-Bi_2O_3 phase, the *IC* dye is degraded to intermediaries by the superoxide radical ($^{\bullet}O^{-2}$) as has been previously reported [29,36].

The relative concentration (C/C_0) of the *IC* dye during dark condition by using the **NB0** and **NB5** solids (Fig. 8B), showed that 22% and 48% of *IC* dye were adsorbed on the solid surface, indicating that the **NB5** solid has high capacity of dye adsorption. During the UV-irradiation (photolysis), the C/C_0 of *IC* dye decreased only 10% in 60 min, whereas by using **NB5** solid, the C/C_0 decreased almost 90% in the same time, indicating apparent high photocatalytic activity. Plotting ln (C_0/C) versus the reaction time (t) yields a straight line (correlation value of 0.996), suggesting that the photodegradation reaction is adjusted to pseudo first order reaction (not shown). From this plot, the

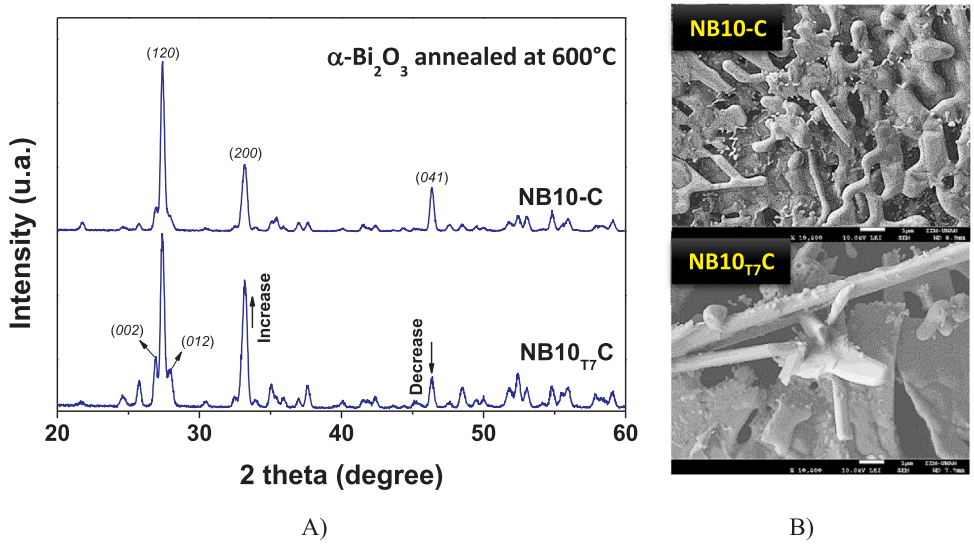

Fig. 7. A) XRD and SEM image of α-Bi_2O_3 annealed at 600 °C from the amorphous solid compounds (**NB10** and **$NB10_{T7}$**) solid.

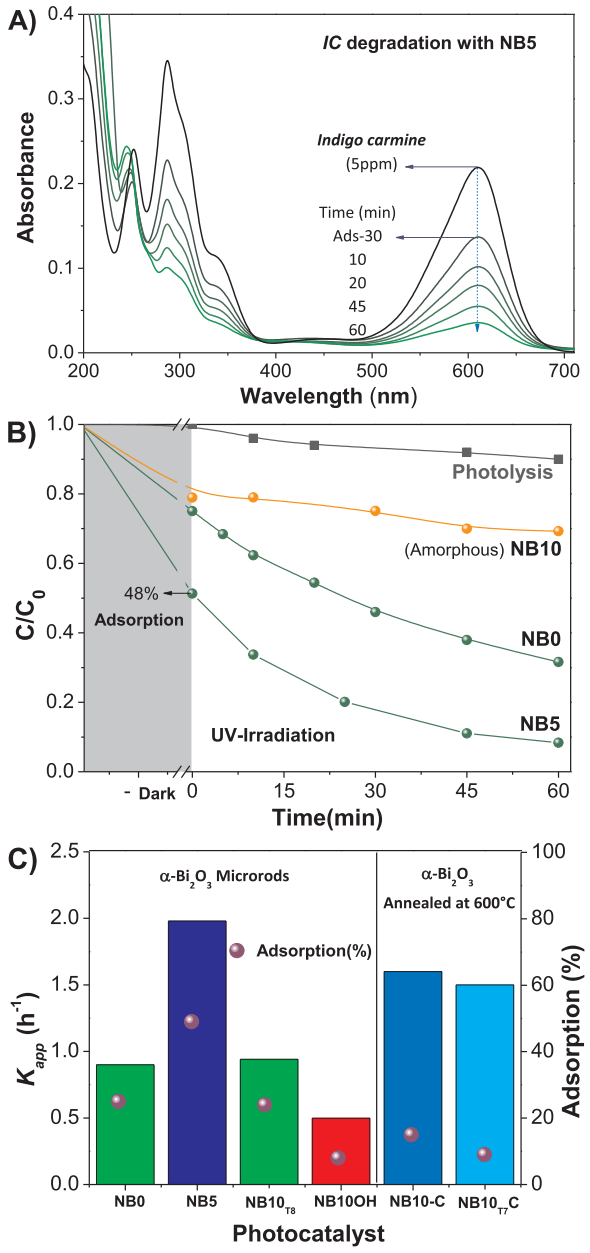

Fig. 8. A) Absorbance spectrum of IC solution using NB5 solid, B) Profile of relative concentration (C/C_0) of IC dye vs time under dark and UV-irradiation, and C) Apparent kinetic rate constant of all microrods α-Bi_2O_3 phase and solids annealed at 600 °C.

apparent kinetic rate constant (K_{app}) of all α-Bi_2O_3 solids can be estimated, and they are shown in Fig. 8C. For the α-Bi_2O_3 microrods prepared in a molar ratio of HNO_3/Bi^{3+} = 5 at 50 °C **(NB5),** its K_{app} value is two times larger than that of the other solids. However, the obtained high value is due to the high adsorption capacity, decreasing 48% the C/C_0 of IC dye in the solution and as consequence the degradation reaction rate is accelerated [36]. Due to difference in the adsorption capacity, it is difficult to determine the real K_{app} of the α-Bi_2O_3 solid. However, it can be seen that all α-Bi_2O_3 microrod solids prepared in *ENH^+-solvent* are more active than that precipitated with OH^- ions (**NB10OH**).

On the other hand, the C/C_0 of *IC* dye using amorphous microsheet compounds is about of 25% (Fig. 8B), and its estimated K_{app} (not shown in the Fig. 8C) is very low (0.24 and 0.35 h^{-1} for **NB10** and **$NB10_{T7}$** solid, respectively). It is expected due to their large bandgap energy (3.2–3.4 eV), which limits their UV-absorption capacity (see Fig. 4A).

By contrast, when these amorphous-compounds are converted to α-Bi_2O_3 phase by annealing at 600 °C (**NB10-C** and **$NB10_{T7}$-C**), their photocatalytic activity is raised (Fig. 8C). Despite their low adsorption capacity, the heterogeneous microsheet-rod-particles of α-Bi_2O_3 phase obtained by annealing exhibited better photocatalytic activity than the microrods (obtained by direct precipitation). The TOC analysis of the irradiated dye solution using **NB10-C or $NB10_{T7}$-C** sample was also investigated. It showed that the total organic carbon in the irradiated solution only decreased 15%, which is in according to the amount of *IC* dye adsorbed in the solid surface. It indicates that the mineralization of the intermediates products originated from *IC* dye was negligible and, therefore, only decolorization/partial degradation of *IC* dye was achieved.

The low activity of as-prepared α-Bi_2O_3 samples can be influenced by the presence of ENH^+ molecule on the solid surface which could affect its interaction with the *IC* dye. By contrast amorphous-compounds, prepared at molar ratio of HNO_3/Bi^{3+} = 10, can lead to α-Bi_2O_3 solids with better photocatalytic response when the ENH^+ molecule is removed after annealing.

3.7. Recyclability test and characterization of re-used Bi_2O_3

It is reported that Bi_2O_3 suffers transformation phenomena during the photocatalytic process under UV irradiation, which could lead to the formation of other oxides such as Bi_2O_{4-x} or to bismuth carbonate ($(BiO)_2CO_3$ or $(BiO)_4CO_3(OH)_2$) in aqueous solution in presence of CO_2, which could affect the photocatalytic properties [37–40]. In order to demonstrate the recyclability of Bi_2O_3 during the photodegradation of *IC* dye under UV-light, **NB0** and **$NB10_{T7}C$** solid were re-used for four cycles of reaction (Figs. 9A and 9B, respectively), using 10 ppm of *IC* dye. The recyclability test revealed that both solids exhibited conversion up to 90% in 2 h during the first cycle. However, the **NB0** solid (Fig. 9A) suffered a 33% deactivation in the second cycle, and then, its photoactivity remained unaltered during the subsequent cycles. The photoactivity of **$NB10_{T7}C$** fell down only 10% after the first cycle and remained constant, suggesting that **$NB10_{T7}C$** solid has larger durability to carry out the *IC* dye degradation. The annealing at 600 °C improved the photostability to the UV-irradiation conditions.

The stability of the re-used Bi_2O_3 solids after the 4 photocatalytic cycles was investigated by XRD and FTIR analysis (Fig. S1A and S1B, respectively). X-ray diffraction of both re-used **NB0** and **$NB10_{T7}C$** solids showed no changes in the patterns comparing to the fresh solids (Fig. 1A and Fig. 7A, respectively), exhibiting reflection peaks characteristic of α-Bi_2O_3 phase without the presence of other compounds. So, reflection peaks of the Bi_2O_{4-x} or $(BiO)_2CO_3$ were not detected, suggesting that Bi_2O_3 was photochemically stable. Similarly, the FTIR spectra showed no significant variations with respect to the fresh solids (Fig. S1B), except for the re-used **$NB10_{T7}C$** solid in which a small band probably corresponding to the stretching vibrations of CO_3^{2-} species was detected. It suggest that CO_3^{2-} species were absorbed on the solid's surface but without formation of the bismuth carbonate.

4. Conclusion

Enlarged microrods α-Bi_2O_3 were directly formed from the bismuth precursor by a simple chemical precipitation method using *ENH^+-solvent* and concentration of nitric acid below of 0.2 M at 50 °C. Using a molar ratio of HNO_3/Bi^{3+} up to 5 and reflux temperature below 70 °C, an amorphous-compound containing ethylenediamine molecule in the structure was obtained. Increasing the entropy energy up to 80 °C led to the conversion of the amorphous-compounds into well crystallized enlarged α-Bi_2O_3 microrods. A relationship between the molar ratio of HNO_3/Bi^{3+} ions and the reflux temperature to induce the direct conversion of either bismuth basic nitrate or amorphous-compounds into α-Bi_2O_3 phase by the precipitation method was demonstrated. The calcination of the amorphous-compounds at 600 °C induced the

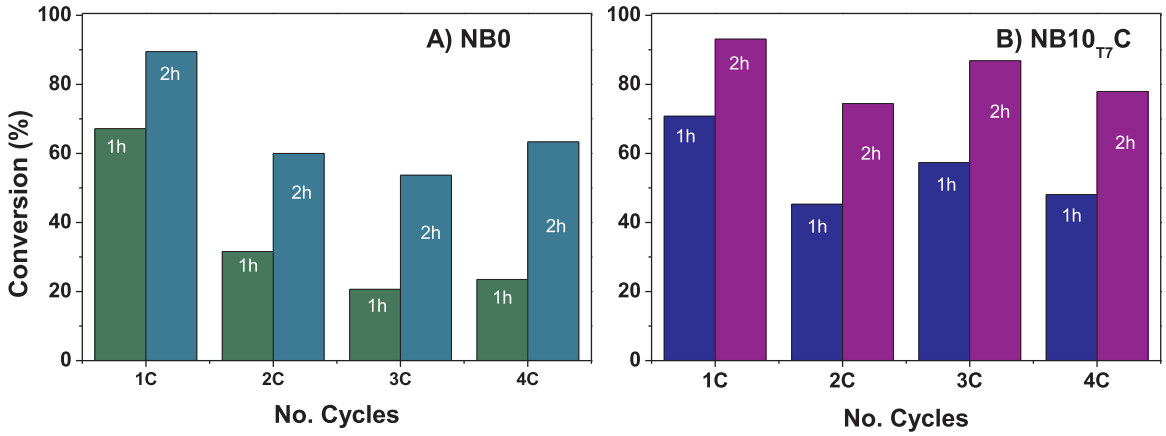

Fig. 9. Profile of the conversion of 10 ppm of *IC* dye at 1 and 2 h of reaction during four cycles, using; A) **NB0** and B) **NB10$_{T7}$C** solids.

elimination of the ethylenediamine molecule and the formation of α-Bi_2O_3 phase. The crystallization of the solids is mainly influenced by the molar ratio HNO_3/Bi^{3+} or HNO_3/ENH^+ ions, and the morphology of α-Bi_2O_3 solid depends on the type of the precipitating agent, the reflux or annealing temperature and the bismuth precursor. Using OH^- ions, the morphology of α-Bi_2O_3 solid resembles short microrods, while larger microrods can be precipitated using ENH^+ ions and moreover, the enlarged microrods are more active for the photocatalytic degradation of the *IC* dye. The results suggest that the enlarged structure of microrods improved the mobility and the electron hole charge separation. Irregular particles of α-Bi_2O_3 phase obtained by annealing of amorphous-compounds, are photochemically stable at least through four cycles of reaction.

Acknowledgments

The author thank to CONACYT for the Catedras-Conacyt/1169. The authors also acknowledge the financial support from CONACYT 251276 and UNAM-PAPIIT IN106015 projects. Finally, the authors recognized the support of A. Tejeda, M.A. Canseco, Eriseth Morales and O. Novelo for making possible the different measurements.

Appendix A. Supporting information

Supplementary data associated with this article can be found in the online version at http://dx.doi.org/10.1016/j.mssp.2018.06.024.

References

[1] T. Lu, Z. Du, J. Liu, H. Ma, J. Xu, Green. Chem. 15 (2013) 2215.
[2] F. Wang, K. Cao, Y. Wu, G.R. Patzke, Y. Zhou, J. Mol. Model. 21 (2015) 48.
[3] S. Park, S. An, H. Ko, C. Lee, J. Nanosci. Nanotechnol. 15 (2015) 1605–1609.
[4] B. Naik, S. Martha, K.M. Parida, Int. J. Hydrog. Energy 36 (2011) 2794–2802.
[5] G. Lin, D. Tan, F. Luo, D. Chen, Q. Zhao, J. Qiu, Z. Xu, J. Alloy. Compd. 507 (2010) L43–L46.
[6] S. Iyyapushpam, S.T. Nishanthi, D. Pathinettam Padiyan, J. Alloy. Compd. 563 (2013) 104–107.
[7] H. Oudghiri-Hassani, S. Rakass, F.T. Al Wadaani, K.J. Al-ghamdi, A. Omer, M. Messali, M. Abboudi, J. Taibah Univ. Sci. 9 (2015) 508–512.
[8] S. Sood, A. Umar, S. Kumar Mehta, S. Kumar Kansal, Ceram. Int. 41 (2015) 3355–3364.
[9] M. Hojamberdiev, G. Zhu, Z.C. Kadirova, J. Han, J. Liang, J. Zhou, X. Wei, P. Liu, Mater. Chem. Phys. 165 (2015) 188–195.
[10] C. Wu, L. Shen, Q. Huang, Y.-C. Zhang, Mater. Lett. 65 (2011) 1134–1136.
[11] H. Lu, S. Wang, L. Zhao, B. Dong, Z. Xu, J. Li, RSC Adv. 2 (2012) 3374.
[12] S. Anandan, J.J. Wu, Mater. Lett. 63 (2009) 2387–2389.
[13] X. Liu, L. Pan, J. Li, K. Yu, Z. Sun, J. Nanosci. Nanotechnol. 13 (2013) 5044–5047.
[14] L.-L. Yang, Q.-F. Han, J. Zhao, J.-W. Zhu, X. Wang, W.-H. Ma, J. Alloy. Compd. 614 (2014) 353–359.
[15] Y. Wang, J. Zhao, B. Zhou, X. Zhao, Z. Wang, Y. Zhu, J. Alloy. Compd. 592 (2014) 296–300.
[16] Y.-C. Wu, Y.-C. Chaing, C.-Y. Huang, S.-F. Wang, H.-Y. Yang, Dyes Pigments 98 (2013) 25–30.
[17] L. Cheng, Y. Kang, J. Alloy. Compd. 585 (2014) 85–93.
[18] R. Yuvakkumar, S.I. Hong, Spectrochim. Acta Part A Mol. Biomol. Spectrosc. 144 (2015) 281–286.
[19] R. Irmawati, M.N. Noorfarizan Nasriah, Y.H. Taufiq-Yap, S.B. Abdul Hamid, Catal. Today 93–95 (2004) 701–709.
[20] Z.-Q. Li, X.-T. Chen, Z.-L. Xue, CrystEngComm 15 (2013) 498–508.
[21] X. Qi, X. Zhu, J. Wu, Q. Wu, X. Li, M. Gu, Mater. Res. Bull. 59 (2014) 435–441.
[22] X. Gou, R. Li, G. Wang, Z. Chen, D. Wexler, Nanotechnology 20 (2009) 495501.
[23] G. Ma, A. Fischer, R. Nieuwendaal, K. Ramaswamy, S.E. Hayes, Inorg. Chim. Acta 358 (2005) 3165–3173.
[24] V. Stavila, R.L. Davidovich, A. Gulea, K.H. Whitmire, Coord. Chem. Rev. 250 (2006) 2782–2810.
[25] Y.-Q. Wu, Y.-L. Qin, C.-R. Li, X.-M. Zhang, Inorg. Chem. Commun. 30 (2013) 133–135.
[26] N. Yang, Y. An, J. Cai, L. Hu, Y. Zeng, Z. Mao, G. Chen, H. Sun, Sci. China Chem. 53 (2010) 2152–2158.
[27] A.J. Ward, A.M. Rich, A.F. Masters, T. Maschmeyer, New J. Chem. 37 (2013) 593–600.
[28] Z.Q. Li, X.T. Chen, Z.L. Xue, J. Colloid Interface Sci. 394 (2013) 69–77.
[29] A. Hernández-Gordillo, J.C. Medina, M. Bizarro, R. Zanella, B.M. Monroy, S.E. Rodil, Ceram. Int. 42 (2016) 11866–11875.
[30] A. Rebhi, T. Makhlouf, N. Njah, Phys. Procedia 2 (2009) 1263–1270.
[31] Y. Wu, G. Lu, Phys. Chem. Chem. Phys. 16 (2014) 4165–4175.
[32] F. Dong, T. Xiong, R. Wang, Y. Sun, Y. Jiang, Dalton Trans. 43 (2014) 6631–6642.
[33] H.-Y. Jiang, P. Li, G. liu, J. Ye, J. Lin, J. Mater. Chem. A 3 (2015) 5119–5125.
[34] Y. Azizian-Kalandaragh, F. Sedaghatdoust-Bodagh, A. Habibi-Yangjeh, Superlattices Microstruct. 81 (2015) 151–160.
[35] Y. Yan, Z. Zhou, Y. Cheng, L. Qiu, C. Gao, J. Zhou, J. Alloy. Compd. 605 (2014) 102–108.
[36] T.A. Gadhi, A. Hernández-Gordillo, M. Bizarro, P. Jagdale, A. Tagliaferro, S.E. Rodil, Ceram. Int. 42 (2016) 13065–13073.
[37] A. Hameed, M. Aslam, I.M.I. Ismail, N. Salah, P. Fornasiero, Appl. Catal. B: Environ. 163 (2015) 444–451.
[38] J. Eberl, H. Kisch, Photochem. Photobiol. Sci. : Off. J. Eur. Photochem. Assoc. Eur. Soc. Photobiol. 7 (2008) 1400–1406.
[39] A. Hameed, V. Gombac, T. Montini, L. Felisari, P. Fornasiero, Chem. Phys. Lett. 483 (2009) 254–261.
[40] A. Hameed, V. Gombac, T. Montini, M. Graziani, P. Fornasiero, Chem. Phys. Lett. 472 (2009) 212–216.